ELSEVIER

Chemical Engineering Journal 135S (2008) S37–S45

Chemical Engineering Journal

www.elsevier.com/locate/cej

Gas–liquid two-phase flow in meandering microchannels

Donata M. Fries, Severin Waelchli [1], Philipp Rudolf von Rohr *

Institute of Process Engineering, Sonneggstrasse 3, ETH Zurich, 8092 Zurich, Switzerland

Abstract

Due to the laminar flow in microfluidic devices, geometrical adaptations are required to enhance the transport across the center line of a microreactor. In gas–liquid segmented flow, the liquid slug between two gas bubbles creates two counter rotating vortices. Using μ-PIV measurements for microchannels with hydraulic diameters of $D_H = 150$ μm and 200 μm, we show that this recirculating movement is very sensitive to the channel geometry. Our results show that the vorticity and swirling strength have the same characteristics before and directly after channel curve. We present the influence of the superficial velocities, channel diameter and curve radius on the recirculating motion. We demonstrate that for segmented gas–liquid flow, an increase of mass transfer over the complete channel diameter is possible by using meandering channels. The flow pattern for straight channels, characterized by two counter rotating vortices symmetrical to the channel center line, changes to two different sized vortices providing strong mass transfer over the center line. Considering these cognitions, we finally propose an optimized mixing design for liquid mixing in a gas–liquid two-phase flow.

Keywords: Gas–liquid flow; Taylor flow; μ-PIV; Curved channel

1. Introduction

Meandering microchannels are desirable as mixers for two reasons: first, they are essential for creating long channels at a small chip size, and second, some special flow effects, providing enhanced mixing, have been observed. Due to the strictly laminar flow regime in microchannels, radial mixing occurs only by diffusion. Various concepts for improved liquid–liquid mixing have been discussed in literature [1,2].

In general, the influence of the curved channel on the flow is completely different for one-phase and two-phase flow. At one-phase flow the so called Dean flow, illustrated at the left side of Fig. 1, is observed for high *Re*, while at two-phase flow asymmetrical recirculations in the Taylor flow regime increase the mass transfer, as can be seen in Fig. 1, right side.

The influence of curved channels on one-phase flow has been numerically investigated by Schönfeld and Hardt [3]. If the flow enters a curve, centrifugal forces create a secondary flow, where mass transfer takes place towards the outer wall of the channel. The fluid is transported back due to recirculation. Note that this recirculation occurs normal to the main flow direction. As a characteristic number for this vortex formation the Dean number $K = Re\sqrt{D_H/r}$ with D_H as hydraulic diameter of the channel and r as the radius of the curve is used. For $K < 200$, the flow is characterized by two counter rotating vortices. At $K > 200$, an additional vortex pair is observed at the outer wall of the channel close to the center line. The vorticity, defined in Eq. (1), increases significantly in this region for $K = 300, \ldots, 400$. Note, that the maximum value of the relative transverse velocity is nearly independent for varying *Re* and *K*.

$$\vec{\omega} = \nabla \times \vec{v} \tag{1}$$

Enhanced mixing due to chaotic advection can be achieved by two strategies: first, a change of the Dean number by changing the curve radius and therefore switching between one and two pairs of counter rotating vortices and second by inverting the channel direction which will change the position of the vortices. These numerical results have been experimentally verified by Jiang et al. [4]. They detected a value of 150 as critical Dean number for switching from the 2 vortices to the 4 vortices. They demonstrated that at higher Dean numbers the mixing length is nearly constant, but due to the increased velocities, the mixing time had been significantly increased. Recently, Sudarsan and Ugaz [5] demonstrated the influence of varying Dean numbers on mixing by spiral channels. They detected a mixing intensity, defined as the ratio between the width of the mixed interface and the width of the channel, of 90% after a channel length

* Corresponding author. Tel.: +41 44 632 24 88; fax: +41 44 632 15 01.
E-mail address: vonrohr@ipe.mavt.ethz.ch (Ph. Rudolf von Rohr).
[1] Present address: ABB Turbo Systems Ltd., Thermal Machinery Laboratory, 5401 Baden, Switzerland.

1385-8947/$ – see front matter © 2007 Elsevier B.V. All rights reserved.
doi:10.1016/j.cej.2007.07.052

Nomenclature

Ca	Capillary number
D_H	hydraulic diameter (m)
j	superficial velocity (m/s)
K	Dean number
r	radius of the channel bend (m)
Re	Reynolds number
T	temperature (°C)
U	velocity component of v in x-direction (m/s)
v	real velocity (m/s)
V	velocity component of v in y-direction (m/s)
$\dot{V}$	volumetric flow rate (m^3/s)
x	flow direction
y	orthogonal to x in the field of view

Greek letters

λ_{ci}	swirling strength ($1/s^2$)
μ	viscosity (Pa s)
ρ	density (kg/m^3)
σ	surface tension (N/m)
ω	vorticity (1/s)
ω_{2D}	vorticity of the 2D-field (1/s)

Subscripts

c	critical value
G	gas phase
L	liquid phase
1	component in x-direction
2	component in y-direction

of 20 mm for Re between $Re = 0.02, \ldots, 18.6$. For a straight channel, the mixing intensity was for all Re below 30% after a length of 20 mm. The mixing intensity at a constant channel length increases with Re for meandering channels and decreases with increasing Re for the straight channels.

The plug formation for immiscible liquid–liquid flow and the recirculation in straight channels have been investigated by Tice et al. [6]. At low Capillary numbers ($Ca < 0.1$) stable plugs with a diameter similar to the channel diameter were formed. Elevated Capillary numbers ($Ca > 1$) lead to smaller droplets. The length of the plug was influenced by the flow rates. The frequency of the plugs seemed to be independent of the flow rates. For straight channels, they observed the recirculation of the left and the right halves. After the plug had moved over a distance equal to its own length, one complete recirculation was observed. After a short time, both halves were mixed, individually but no mixing of the complete plug was observed. Song et al. [7] investigated this recirculation for winding channels: even at low Re ($Re < 10$) the plug in a curve moves at different velocities relative to the channel walls. Therefore, the symmetry is broken and mass transfer between both halves was observed. This results in a significant increase of mixing.

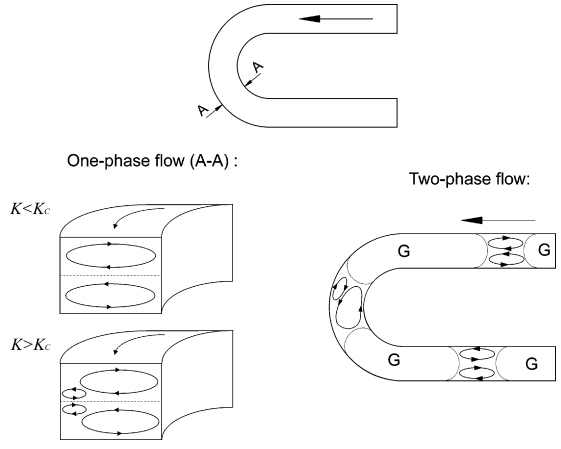

Fig. 1. Schematic flow effects in meandering channels for one-phase flow (left side), and two-phase flow (right side).

The flow patterns and flow characteristics for gas–liquid two-phase flow, focused on the segmented flow pattern in straight microchannels for different liquids, had been investigated by Waelchli and Rudolf von Rohr [8]. The recirculation is symmetrical to the channel center line; the vortex center of the counter rotating eddies was found to be close to the channel wall.

Guenther et al. [9,10] investigated the influence of channel bending on mixing of miscible liquids in gas–liquid segmented flow. At straight channels with a cross-section of 400 μm × 150 μm, they obtained a recirculation inside the liquid slug symmetrical to the channel center line. In a channel bend with a bending radius of 600 μm, this recirculation was observed to be a non-symmetric one. Inside the recirculating liquid elements, velocities normal to the channel wall of approximately 30% of the bulk liquid velocity were observed. Mixing experiments demonstrated a decreased mixing length (ratio of the channel length to achieve a standard deviation of the intensity equal to 10% of the original value and the hydraulic diameter of the channel) by a factor of 5 by use of meandering channels compared to a straight channel. They operated at low Capillary numbers of $Ca < 0.02$ and very low superficial velocities by the gaseous ($j_G = 8$ mm/s) and the liquid phase ($j_L = 3$ mm/s).

In this study, we focus on the segmented gas–liquid two-phase flow (also named intermittent flow or Taylor flow), because, in contrast to the bubbly flow and the annular flow pattern, this flow pattern provides enhanced mixing in the liquid slug by the two counter rotating vortices. Since this recirculating movement in straight channels provides no mixing over the complete microchannel, we investigate the vortex characteristics of Taylor flow in meandering channels for moderate velocities in both phases ($j_L = 40, \ldots, 70$ mm/s, $j_G = 370, \ldots, 740$ mm/s). Keeping the channel height constant at 150 μm, we vary the channel width (150 μm and 300 μm) and the bend radius (1200 μm and 600 μm). We compare the liquid flow distribution directly before entering, after leaving a channel bend and while passing a meandering channel. Based on the results reported in literature and obtained by our experiments, we will propose some general design rules to enhance the non-symmetric velocity field in the slug by meandering channels.

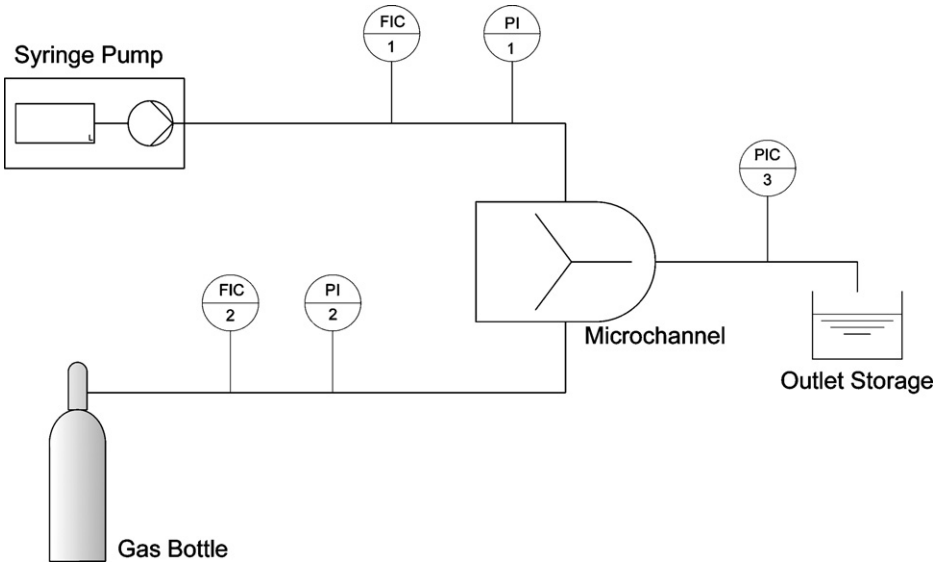

Fig. 2. Scheme of the experimental setup used.

2. Experimental

The microreactors were fabricated via standard photolithograhical processes. The design of the channel has been created via CAD-programmes and was printed with high resolution (2400 dpi) on the mask. A double-side polished silicon wafer (4 in. diameter, 525 μm thickness) was cleaned (10 min ultrasonic acetone bath followed by 10 min ultrasonic isopropanol bath, then rinsing with deionized water and finally treated in an oxygen plasma) and covered with 10 μm thick layer of positive photoresist (AZ 4562, Clariant) by spin-coating. After the exposure and development, the channels have been formed by reactive ion etching. This procedure had been repeated for the wafer backside to obtain the inlet- and outlet-holes. The patterned silicon wafer was sealed to a glass wafer by anodic bonding. Each wafer contained six microchannels. They were separated after the bonding process by a wafer saw. The microchannels have a rectangular cross-section, characterized by the width and the height of the channel. For this experimental study, we used reactors with a width 150 μm and 300 μm of and a height of 150 μm for all reactors.

A scheme of the experimental setup is given in Fig. 2. The liquid phase (water colored with Rhodamine B, concentration $c_{Rh} = 5 \times 10^{-6}$ mol/l, for details see Table 1) was stored in a syringe. Pumping and controlling of the flow rate was performed via a syringe pump (Harvard Apparatus, accuracy within 0.35%, reproducibility within 0.05%). The gas phase (nitrogen, see Table 1) was delivered from a gas bottle; the flow rate was controlled via a flow controller (Bronkhorst, accuracy ±0.5%). The tubing and connections to the reactor were realized with PEEK elements (Upchurch). All experiments were performed at a constant room temperature of $T = 20\,^{\circ}C$.

Table 1
Properties of the used fluids, $T = 20\,^{\circ}C$

	Density ρ (kg/m^3)	Viscosity η (mPa s)	Surface tension σ (mN/m)
Deionized water	1032	1.025	75.54
Nitrogen	1.1508	0.01732	–

Visualization of the flow was realized via an inverted fluorescence microscope (Zeiss Axiovert 200), equipped with a Rhodamine B filter set and with a dual-frame low noise CCD-Camera (PCO SensiCam QE, 5 dual-frames per second, 1376 pxl × 1040 pxl). Depending on the used objective, the field of view was 1.65 mm × 1.24 mm (5×) and 0.82 mm × 0.62 mm (10×). A pulsed Nd:YAG laser (La Vision) was used for illumination. A commercial timing unit (La Vision) synchronized the laser shots and the camera frames. The time delay between both frames within one double-exposed micrograph was 100 μs for the μ-PIV measurements. The measured field is defined by a small depth-of-field of the 1.25 lens. Given a criteria of less than 25% increase in particle diameter, the depth-of-field for the present system was measured to be 1.1 μm. Particles outside this field are at least 25% enlarged to the particles in the focal plane and have therefor lower intensity values.

3. Data analysis

The liquid flow distribution was analyzed using micron-resolution particle image velocimetry (μ-PIV). As tracer particles red fluorescent polymer spheres with a diameter of 1 μm (Duke Scientific Corporation) were used. The vector field was calculated by a cross-correlation algorithm of the double-exposed micrographs. The vector plots, vorticity values, swirling strength and the streamlines were calculated using the commercial software DaVis 6 (La Vision). Except for the measurements directly in the channel bend, 200 micrographs were averaged for statistical reasons. A detailed explanation of the used method is given in [8].

To characterize the recirculation in the liquid velocity field, the vorticity and swirling strength were analyzed. The vorticity,

defined in Eq. (1), can be rewritten for the two-dimensional case as:

$$\omega_{2D} = \frac{\partial v}{\partial X} - \frac{\partial u}{\partial Y} \tag{2}$$

and detects the internal recirculation motion as well as shear strain. Note, that ω_{2D} is one component of the vector $\vec{\omega}$, which can be illustrated as a scalar. A positive value of ω_{2D} indicates a counter-clockwise rotation, a negative value of the vorticity a clockwise rotation. In the following, ω_{2D} is named vorticity.

As shear strain in microchannels cannot be neglected due to the strong wall effects, an additional method for analyzing the rotation is advantageous. The swirling strength, derived from the critical point analysis of the local velocity gradient tensor ∇v, has been used for characterizing the recirculation motion. The swirling strength λ_{ci} is the complex part of the eigenvalue of

$$\nabla v = \begin{bmatrix} \frac{\partial v_1}{\partial x} & \frac{\partial v_1}{\partial y} \\ \frac{\partial v_2}{\partial x} & \frac{\partial v_2}{\partial y} \end{bmatrix} \tag{3}$$

and identifies regions with a local swirling motion. In contrast to the vorticity, the swirling strength contains no information about the direction of the rotation. In this study, we analyzed the vorticity of the two-dimensional vector field as well as the swirling strength.

4. Results and discussion

4.1. Comparison of the hydrodynamics before and after the bend

Figs. 4–7 characterize the liquid slug motion before entering (Position 1, see Fig. 3) and after leaving (Position 2, see Fig. 3) the channel curve. The relative velocity vectors (difference between the absolute velocity and the bulk velocity) together with the liquid vorticity are shown in the top comparison. The swirling strengths are depicted in the center, whereas the streamlines of the two configurations can be seen at the bottom. Note, that due to the turning of the channel the channel outer wall changes from the top border on the left side (before the channel bend) to the bottom border on the right side (after the channel bend). Although the vorticity is dominated by the shear stress, the two counter rotating vortices and the symmetry axis at the channel center, where the vorticity is zero, can be detected in all vorticity plots (see Figs. 4–7, top comparison). Additionally, small vortices counter rotating to the main recirculation movement near the gas bubble have been observed. These places of slightly increased vorticity cannot be identified in the swirling strength plot, indicating either that they are dominated by the shear stress or being too small. The latter one seems to be the reason, further investigations are required to confirm this assumption. The situation before entering the bend and after leaving the bend is comparable to that in straight channels, as it had been analyzed by Waelchli and Rudolf von Rohr [8]. This indicates, that for this configuration a few millimeters channel length creates the characteristic flow. The recirculating movement seems to be very sensitive to a change of the flow direction. A comparison of the performed experiments is given in Figs. 4–7 is given in Table 2.

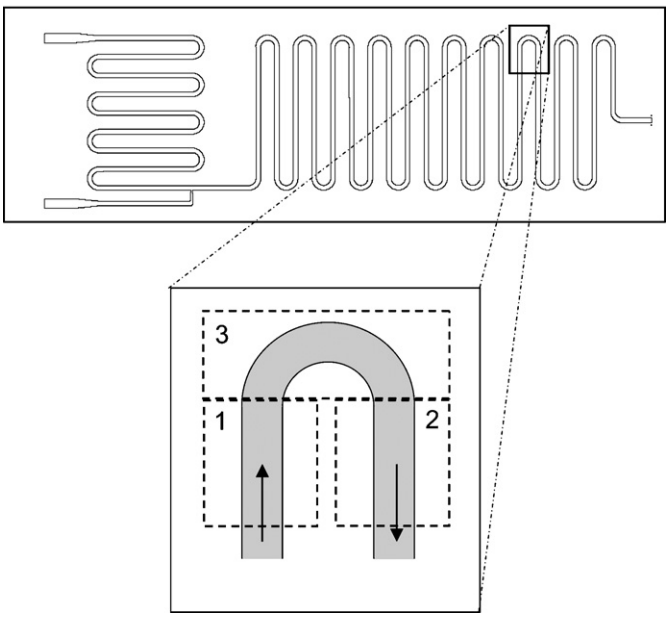

Fig. 3. Reactor design with locations of the recirculation measurements.

The "reference channel" is characterized by a hydraulic diameter of $D_H = 150\ \mu m$, and a channel radius of $r = 1.2$ mm. In Fig. 4, the hydrodynamic properties for this channel at superficial velocities of $j_G = 0.37$ m/s and $j_L = 0.04$ m/s are depicted as "reference case". The vorticity shows the same characteristics before and after the channel bend. A slight decrease of the vorticity maximum value can be observed, indicating a marginal pressure drop. The vortex-free region, indicated by a vorticity of zero, is before and after the channel bend identical with the channel center line. The swirling strength, presented in the middle of Fig. 4, shows the same trends like the vorticity: a small decrease of the maximum of the recirculating movement denotes the pressure drop. Comparing the streamlines before and after the bend identifies an insignificant asymmetry. A real break up of the symmetry could not be identified. Additionally, a small elongation of 15% of the liquid slug length is observed.

Increasing the superficial velocities gives the same trends. In Fig. 5 the flow characteristics are illustrated for a microreactor with a hydraulic diameter of $D_H = 150\ \mu m$ and superficial velocities of $j_G = 0.74$ m/s and $j_L = 0.07$ m/s. The observed changes in

Table 2
Experiments on the liquid slug motion before and after the channel bend

	Fig. 4	Fig. 5	Fig. 6	Fig. 7
w (μm)	150	150	300	150
h (μm)	150	150	150	150
r (mm)	1.2	1.2	1.2	0.6
j_L (m/s)	0.04	0.07	0.04	0.04
j_G (m/s)	0.56	0.74	0.37	0.56

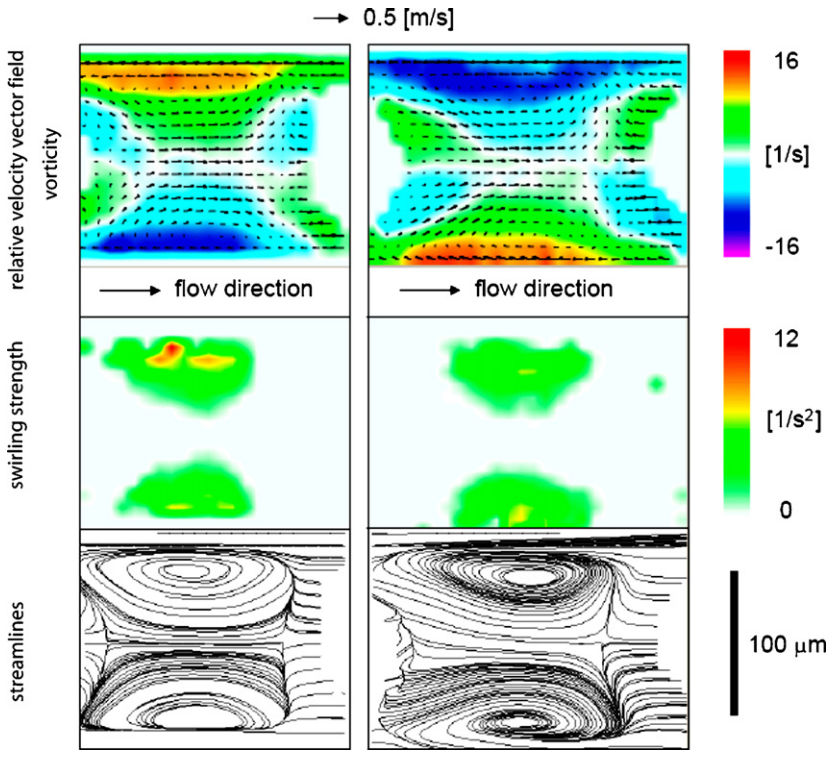

Fig. 4. Characteristics of two liquid plugs entering (left) and leaving (right) a microchannel bend ($r = 1.2$ mm) for a channel with $D_H = 150$ µm and a fluid system with $j_G = 0.56$ m/s ($\dot{V}_G = 0.75$ ml/min) and $j_L = 0.04$ m/s ($\dot{V}_L = 0.05$ ml/min).

the hydrodynamic properties are identical to the results with the smaller velocities in the same channel geometry (Fig. 4): the vorticity and the swirling strength decrease by passing the channel. The streamlines are before and after the channel bend symmetrical to the channel center line. As for the lower velocities, an elongation of the liquid slug of approximately 15% can be identified. The maximum value of the vorticity and the swirling strength are the same for the small and the increased superficial

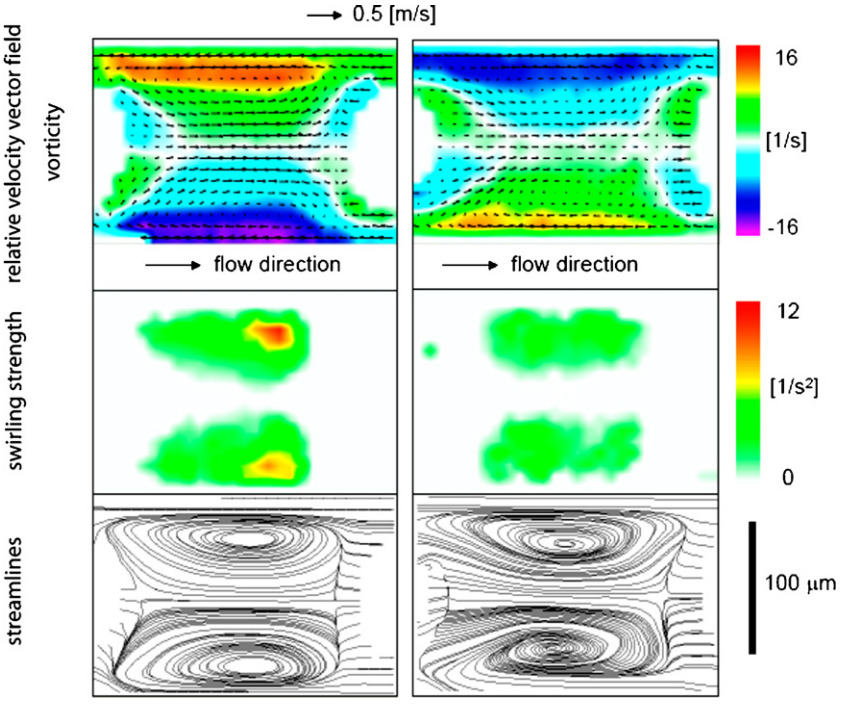

Fig. 5. Characteristics of two liquid plugs entering (left) and leaving (right) a microchannel bend ($r = 1.2$ mm) for a channel with $D_H = 150$ µm and a fluid system with $j_G = 0.74$ m/s ($\dot{V}_G = 1$ ml/min) and $j_L = 0.07$ m/s ($\dot{V}_L = 0.1$ ml/min).

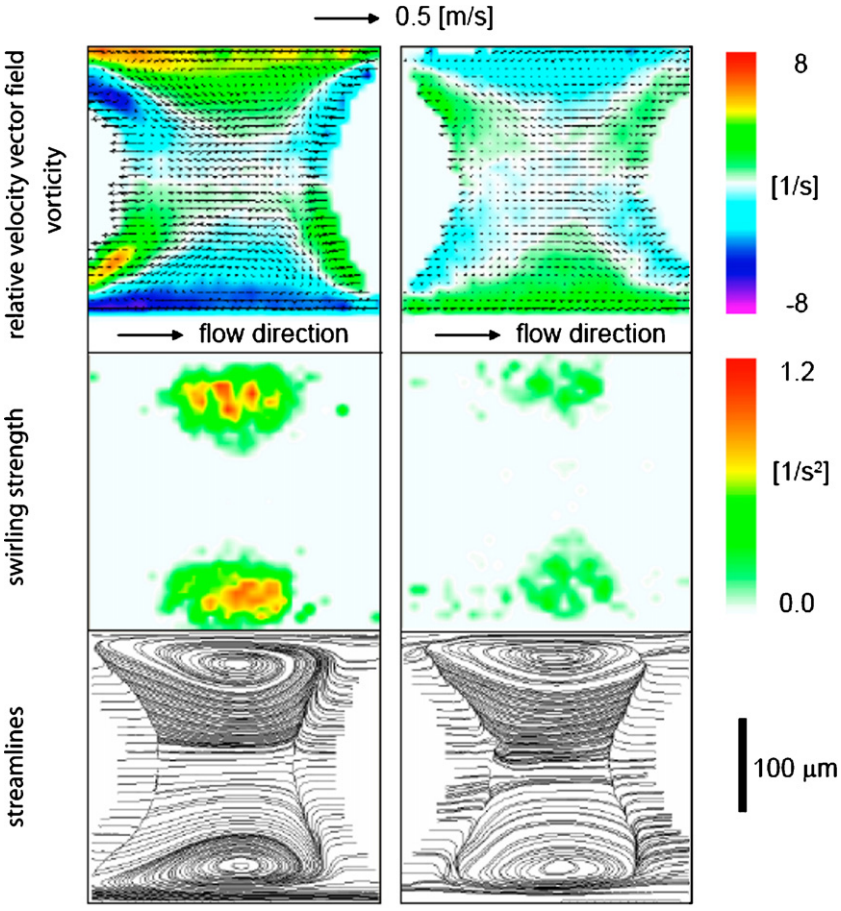

Fig. 6. Characteristics of two liquid plugs entering (left) and leaving (right) a microchannel bend ($r = 1.2$ mm) for a channel with $D_H = 200$ µm and a fluid system with $j_G = 0.37$ m/s ($\dot{V}_G = 1$ ml/min) and $j_L = 0.04$ m/s ($\dot{V}_L = 0.1$ ml/min).

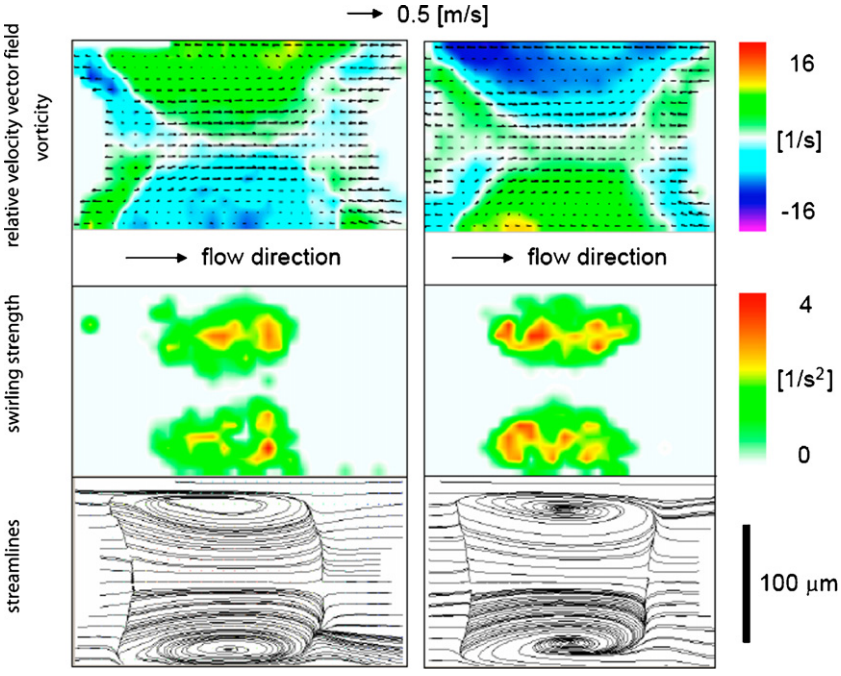

Fig. 7. Characteristics of two liquid plugs entering (left) and leaving (right) a microchannel bend ($r = 0.6$ mm) for a channel with $D_H = 150$ µm and a fluid system with $j_G = 0.56$ m/s ($\dot{V}_G = 0.75$ ml/min) and $j_L = 0.04$ m/s ($\dot{V}_L = 0.05$ ml/min).

velocities, but the area of higher vorticity and swirling strength is increased for the increased velocities.

In order to prove the influence of the hydraulic diameter, we performed experiments in a rectangular microchannel with $D_H = 200$ μm and a radius of the bend of $r = 1.2$ mm. The ratio of the superficial gas and the superficial liquid velocities is again 10:1, the superficial gas velocity is $j_G = 0.37$ m/s. Therefore the superficial velocities are the similar to those in the reference case (see Fig. 4). The results for the increased channel diameter can be seen in Fig. 6. Again, the comparison of the flow before and after the channel bend shows a decreased vorticity and swirling strength behind the bend, caused by a slight pressure drop in the channel bend. The velocities seem to be more uniform compared to those before the bend. The symmetry of the recirculation towards the center line is only slightly decreased. In contrast to the experiments with the smaller channel diameter, no elongation of the liquid slug length can be detected.

Comparing with the $D_H = 150$ μm-microchannel (see Fig. 4), indicates a decrease of the vorticity and the swirling strength. As the superficial velocities are the similar, the influence of the wall on the recirculation seems to be more dominant compared to the influence of the superficial velocity.

In order to detect the influence of the radii, we decreased the curve radii from 1.2 mm to 0.6 mm. The hydraulic diameter of the channel is $D_H = 150$ μm, the superficial velocities are identical with the reference case, $j_G = 0.56$ m/s and $j_L = 0.04$ m/s. As can be seen in Fig. 7, no decrease in the vorticity and swirling strength can be detected. The maximum value of the swirling strength is similar to the one before the bend, but the area of higher swirling strength values is increased compared to the situation before the bend. The absolute values of the swirling strength are decreased compared to those for the larger radii, compare Fig. 4. The vorticity seems to be decreased for increasing curve radii. No significant elongation of the liquid slug length is observed. In contrast to the reference case, the vorticity shows decreased maximum values, but the vorticity inside the vortex is nearly constant. The swirling strength has a more enlarged area of high values (>2 1/s^2) than the reference channel at the same superficial velocities but larger curve radius. A decrease of the curve radius seems to enhance the recirculating movement.

4.2. Situation inside the bend

Since the observations before and after the channel bend are in contrast to the results to be expected after the literature review, and to explain the observed elongation of the liquid slug when passing the bend, we investigated the flow behaviour directly in the bend for two different superficial velocities in the reference microchannel ($D_H = 150$ μm, $r = 1.2$ mm). The similarity of the liquid slug before and after the bend leads to the assumption that increased velocities at the outer half of the channel result in a velocity gradient across the center line. This would lead to the expected mass transfer across the channel line in the bend.

Figs. 8–10 show that a strong relative motion diagonally through the liquid slug occurs after a short inlet zone (turning angle of approximately 45°), resulting in a strong mass transfer across the center line and a symmetry break up (c–e). This

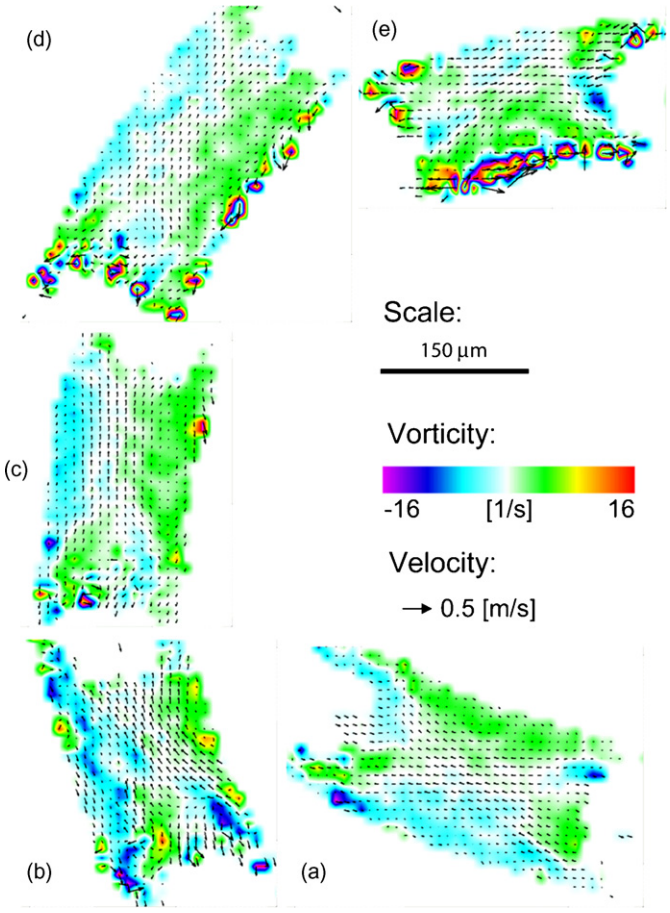

Fig. 8. Instantaneous relative velocity distributions and vorticity contours for liquid plugs in a microchannel with $D_H = 150$ μm and radius $r = 1200$ μm. The superficial velocities were $j_G = 0.56$ m/s and $j_L = 0.04$ m/s. The two-phase flow is flowing clockwise.

mass transfer across the channel center line is visible in the vector plot and in the vorticity layer: the contact line between both vortices, indicated by a vorticity of zero, moves away from the middle of the channel when entering the bend (see part (a) in Figs. 8–10) to a diagonal line from the channel inner wall at the end of the plug to the channel outer wall at the front of the plug (see part (d and e) in Figs. 8–10) when leaving the channel bend. The vortex at the outer half of the bend is nearly zero, whereas the vortex at the inner half is located near the gas bubble trailing end. Since these figures are derived from instantaneous measurements, for statistical reasons no swirling strength and streamline has been calculated. At increased superficial velocities (see Fig. 9), the detected vorticity and the measured relative velocities are also increased. The mass transfer in the channel bend seems to be independent of the superficial velocities, the area with the vorticity of zero has the same geometry for lower superficial velocities (Fig. 8) and for elevated superficial velocities (Fig. 9).

Decreasing the curve radius shows the same trends, see Fig. 10. The vorticity is similar to that in the reference channel at same velocities (Fig. 8). The inlet zone for the mass transfer across the channel line is slightly enlarged (approximately 90°) but is strongly developed at the outlet.

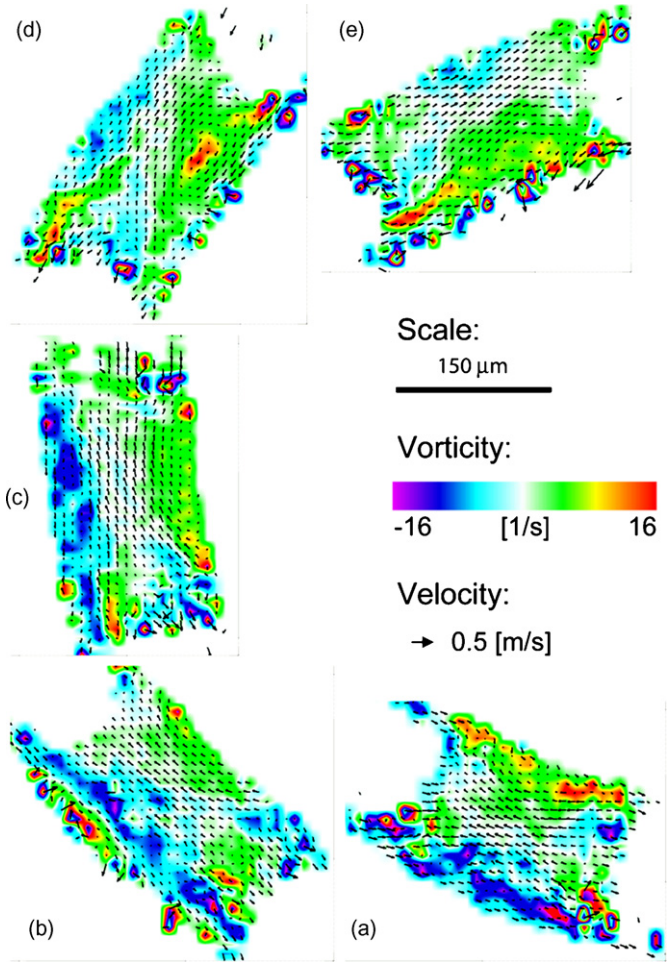

Fig. 9. Instantaneous relative velocity distributions and vorticity contours for liquid plugs in a microchannel with $D_H = 150$ µm and radius $r = 1200$ µm. The superficial velocities were $j_G = 0.74$ m/s and $j_L = 0.07$ m/s. The two-phase flow is flowing clockwise.

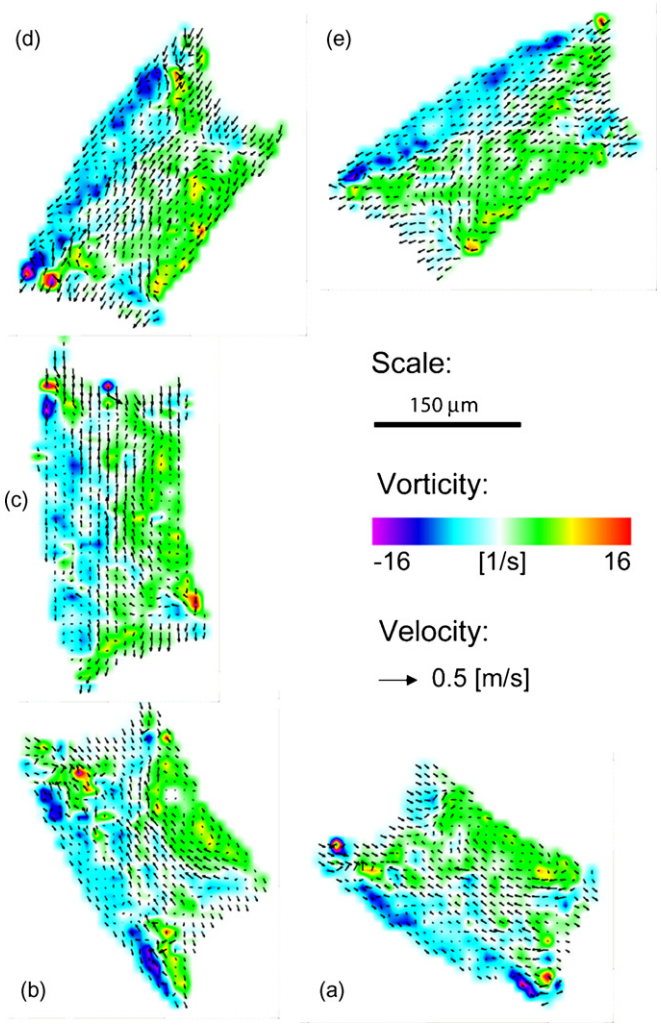

Fig. 10. Instantaneous relative velocity distributions and vorticity contours for liquid plugs in a microchannel with $D_H = 150$ µm and radius $r = 600$ µm. The superficial velocities were $j_G = 0.56$ m/s and $j_L = 0.04$ m/s. The two-phase flow is flowing clockwise.

Analyzing the wall normal and the streamwise component of the average velocity in dependence of the position of the liquid slug center in the channel bend (turning angle), as it had been done in Fig. 11 for the reference case, indicates an increase of the average wall normal velocity component and a decrease of the average streamwise component. In other words, this means a loss of symmetry and therefore an increased mass transfer motion across the channel center line. We state that this mass transfer motion across the channel center line increases with the turning angle. Note, that the exact plug position (turning angle) is difficult to measure. The accuracy of the given angle is $\pm 2^\circ$. Due to the precise time management and the adjusted algorithm in finding the cross-correlation, the uncertainty of these values is below 5%.

4.3. Design rules

Based on these results, we propose some design rules to enhance the recirculating movement over both channel halves in the liquid slug. In general, for strong recirculating movement by optimized channel design complete turnings or even

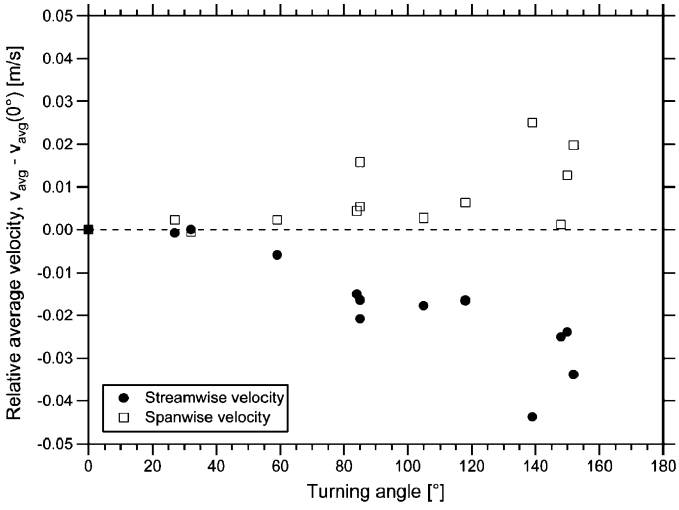

Fig. 11. Average spanwise (wall normal, transfer motion) and streamwise velocity component inside the liquid slug relative to the velocities in a straight microchannel depending on the liquid slug position (turning angle).

270°-curves are advantageous. Furthermore the turning radius should be small. For increased vortices across the channel center line in the bend increased superficial velocities are preferable. At given flow rate, a decrease of the hydraulic diameter provides an enhanced mass transport. A critical ratio of curve radii, channel diameter and velocities, as is the Dean number for one-phase flow, is not known. Although the recirculating movement of the one-phase flow is completely different to the gas–liquid two-phase flow, the design ideas can be adapted: increasing the centrifugal force by decreasing the curve radius and increasing the superficial velocities.

5. Conclusion

We demonstrate that the liquid velocity field in segmented gas–liquid flow depends on the channel geometry and the superficial velocity rates. When passing the channel bend, liquid is transported due to centrifugal forces from the inner channel halve to the outer one and transported back by the recirculation. This asymmetric motion can be enhanced by increasing the superficial liquid velocities. After leaving the channel bend, the liquid velocity profile is similar to the one before entering the bend, indicating, that the flow is very sensitive to the channel geometry. The swirling strength before and after a channel curve at constant velocity rates can be decreased by increasing curve radii and using smaller channel diameters. As general design rules for an optimized recirculation across the channel center line in the liquid slug segments in gas–liquid two-phase flow we advise a large turning angle, a small turning radius and a small hydraulic diameter, resulting in higher velocity rates. The influence of this asymmetrical flow on the mass transfer, e.g. the mixing length will be proven in the future.

Acknowledgements

The authors wish to thank the ETH Research Grant and the Emil-Barell-Foundation for financial support.

References

[1] S. Hardt, K.S. Drese, V. Hessel, F. Schönfeld, Passive micromixers for applications in the microreactor and μTAS fields, Microfluid Nanofluid 1 (2) (2005) 108–118.
[2] N.-T. Nguyen, Z. Wu, Micromixers—a review, J. Micromech. Microeng. 15 (2) (2005) R1–R16.
[3] F. Schönfeld, S. Hardt, Simulation of helical flows in microchannels, AIChE J. 50 (4) (2004) 771–778.
[4] F. Jiang, K.S. Drese, S. Hardt, M. Küpper, F. Schönfeld, Helical flows and chaotic mixing in curved micro channels, AIChE J. 50 (9) (2004) 2297–2305.
[5] A.P. Sudarsan, V.M. Ugaz, Fluid mixing in planar spiral microchannels, Lab Chip 6 (1) (2006) 74–82.
[6] J.D. Tice, H. Song, A.D. Lyon, R.F. Ismagilov, Formation of droplets and mixing in multiphase microfluidics at low values of the Reynolds and the Capillary numbers, Langmuir 19 (22) (2003) 9127–9133.
[7] H. Song, J.D. Tice, R.F. Ismagilov, A microfluidic system for controlling reaction networks in time, Angew. Chem. Int. Ed. 42 (7) (2003) 767–772.
[8] S. Waelchli, P. Rudolf von Rohr, Two-phase flow characteristics in gas–liquid microreactors, Int. J. Multiphase Flow 32 (7) (2006) 791–806.
[9] A. Guenther, S.A. Khan, M. Thalmann, F. Trachsel, K.F. Jensen, Transport and reaction in microscale segmented gas–liquid flow, Lab Chip 4 (2004) 278–286.
[10] A. Guenther, M. Thalmann, M. Jhunjhunwala, M.A. Schmidt, K.F. Jensen, Micromixing of miscible liquids in segmented gas–liquid flow, Langmuir 21 (4) (2005) 1547–1555.